

Explaining 3D Computed Tomography Classifiers with Counterfactuals

Joseph Paul Cohen[†]
Stanford University

JOSEPH@JOSEPHPCOHEN.COM

Louis Blankemeier
Stanford University

Akshay Chaudhari
Stanford University

Abstract

Counterfactual explanations in medical imaging are critical for understanding the predictions made by deep learning models. We extend the Latent Shift counterfactual generation method from 2D applications to 3D computed tomography (CT) scans. We address the challenges associated with 3D data, such as limited training samples and high memory demands, by implementing a slice-based approach. This method leverages a 2D encoder trained on CT slices, which are subsequently combined to maintain 3D context. We demonstrate this technique on two models for clinical phenotype prediction and lung segmentation. Our approach is both memory-efficient and effective for generating interpretable counterfactuals in high-resolution 3D medical imaging.

1. Introduction

Neural Networks can learn to identify features and make predictions from computed tomography (CT) scans predicting clinical phenotypes (Blankemeier et al., 2024) and survival (Thanoon et al., 2023). To understand why these predictions are made, it is crucial to have interpretable explanations, especially in the medical domain where high-stakes decisions are made. Synthetic counterfactual CT volumes can be created to simulate a change in the class label of an image, providing insights into the factors influencing the model’s predictions.

In this work we extend the counterfactual generation method of Latent Shift, previously demonstrated for 2D counterfactuals (CFs) (Cohen et al., 2021), into the 3D domain to enable it to work for CT volumes. While a natural approach would be to use a 3D autoencoder, this presents difficulties such as the scarcity of training data for 3D autoencoders and the significant computational and memory demands, especially for large models and high-resolution data, both of which are likely required for generating high-quality counterfactuals.

To address this, we employ a 2D autoencoder by slicing the 3D volumes, then encoding, decoding, and concatenating the slices. This slice-based approach is more data-efficient than training directly on entire volumes, helping to mitigate overfitting by avoiding biases related to specific acquisition views (e.g., abdomen or head). By randomly sampling slices, the model is less likely to learn unwanted correlations connected to particular views.

[†]Work not related to position at Amazon.

Challenges posed by memory constraints on GPUs persist, particularly when calculating a partial derivative with respect to the latent space, preventing counterfactual generation for entire volumes. To address this the gradient is propagated for only a subset of the slices which limits where in the volume the changes can be made. Our findings indicate that this approach minimally affects the effectiveness of the generated counterfactuals.

Contributions:

- Train a VQ-GAN on 1,447,551 slices from 12,686 CT scans to enable CF generation.
- Develop a memory-efficient approach to generate CFs with limited GPU memory.
- Study two prediction models: one for clinical phenotype prediction and another for lung segmentation.

2. Counterfactual Generation

The Latent Shift method (Cohen et al., 2021) is employed to generate counterfactuals (CFs). In order to make modifications to the image this method requires computing the gradient from the output of the classifier to the latent space of an autoencoder $\frac{\partial f(D(E(x)))}{\partial z}$ where $z = E(x)$. E and D are an encoder/decoder pair trained to represent the domain of CT Scans (see §3). This gradient is then subtracted from the latent representation of the input image with a coefficient λ . The coefficient λ is selected to ensure a predetermined change in the classifier’s output.

Computing this gradient is memory-intensive, particularly when using a 3D classifier and autoencoder. In order to make this tractable, a 2D autoencoder is used which allows us to propagate the gradient to only a subset of slices, and their respective latent embeddings. We call this approach Slice AE and depict it in Figure 1. With this approach the entire volume is encoded slice by slice and then decoded and concatenated into a full volume and input into the classifier. During decoding, gradients are computed for only a subset of slices. The remaining slices have the gradient blocked. This approach allows the classifier to compute gradients for a few slices without sacrificing the context of the entire volume. Typically only 10 slices can have their gradient computed using 32GB of memory on a Tesla V100 used for this work.

This gradient can then be used to modify the latent representation and then decoded and concatenated and input into the classifier to determine if the the prediction has been sufficiently reduced. An iterative search is used by reducing the value of λ until the prediction stops decreasing.

3. Model and Training

We train a VQ-GAN (Esser et al., 2021) which is a VQ-VAE (vector quantized variational autoencoder) with a perceptual adversarial loss. This approach generates high-resolution images while having an encoder/decoder which provides a latent space that can be navigated using CF generation methods. This is in contrast to diffusion models which also generate high-resolution images but the latent space requires iterations, so it is not trivially compatible with existing CF generation methods.

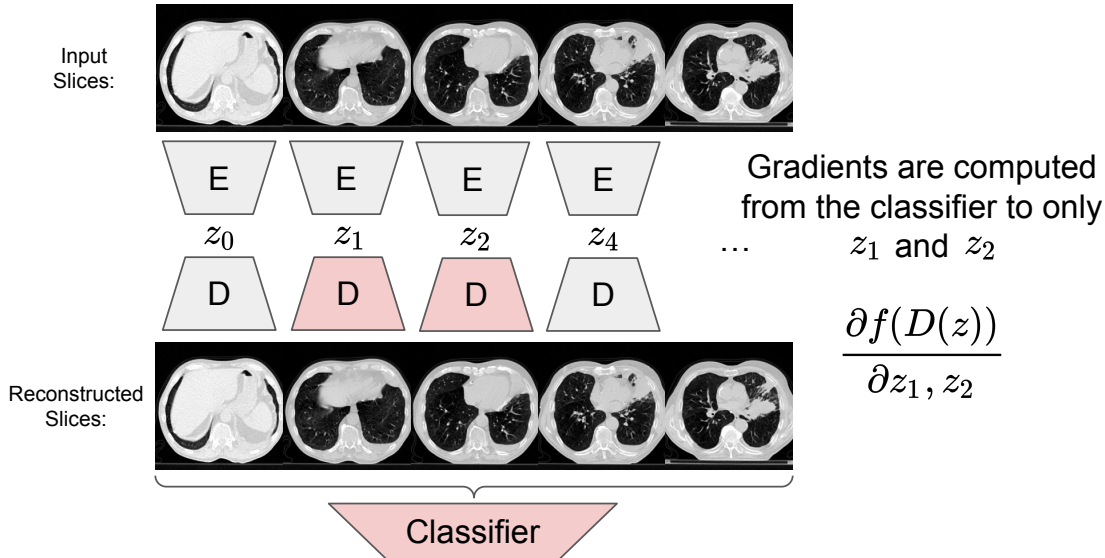


Figure 1: Illustration of the slice-based autoencoder (Slice AE) approach for generating counterfactuals in 3D CT volumes. Only selected latent representations, z_1 and z_2 , have gradients computed from the classifier output, enabling memory-efficient counterfactual generation while preserving the ability to navigate and modify specific parts of the 3D volume.

This model is used to reconstruct at the slice level instead of the entire volumes. This is done for data efficiency as volumes are very high dimensional and don't always capture the same extent, which would likely lead to overfitting. To further maximize data efficiency, images are scaled down by 1/2 (often 512x512 \rightarrow 256x256) and the model is trained on crops of 128x128. Training on crops enables the use of volumes that have already been cropped from a larger volume, which is commonly found in public datasets. This allows the model to observe multiple organs at once in the receptive field. Code and model weights in PyTorch (Paszke et al., 2019) are available online*.

4. Data

The study utilizes three datasets selected for their size, public availability, coverage of various organ systems, and inclusion of both healthy and diseased states. The LUNA16 dataset (Setio et al., 2016) contains imaging data focused on the lungs and includes cancerous lesions. A total of 227,225 slices were obtained from 888 volumetric scans. The TotalSegmenter dataset (Wasserthal et al., 2022) provides imaging of all major organs, with 312,400 slices obtained from 1,204 scans. The DeepLesion dataset (Yan et al., 2017) includes images of multiple organs, both healthy and with lesions, offering a robust representation of diseased tissues. From 10,594 scans, 907,926 slices are obtained. Collectively, these datasets ensure comprehensive representation of both healthy and unhealthy organs, contributing to providing a good data representation to the model.

*Code and model weights available: <https://github.com/ieee8023/ct-counterfactuals>

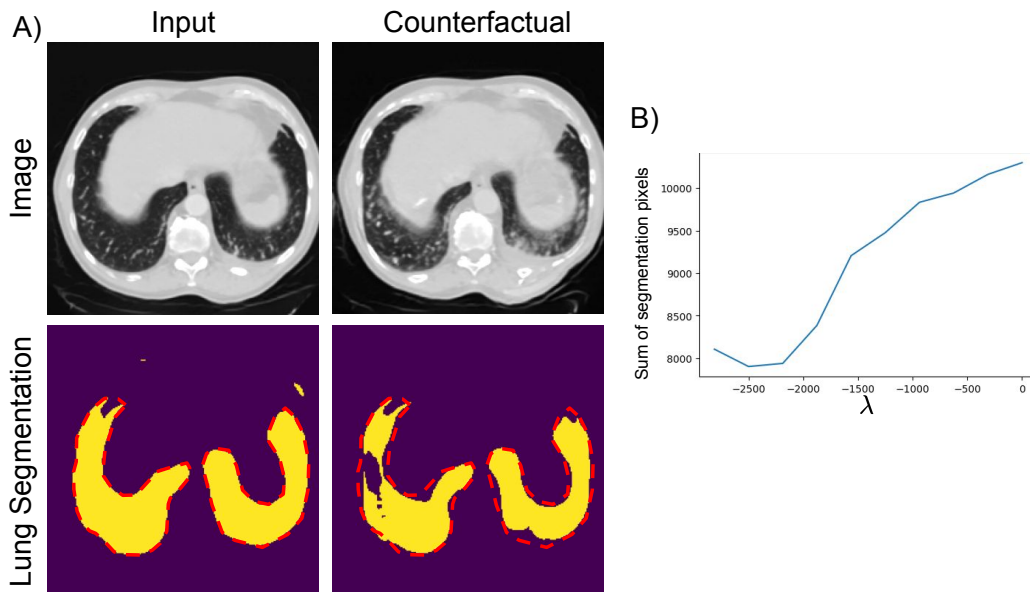


Figure 2: A) An example CF generated for lung size. The model’s predicted segmentation mask for lung is shown below. A red outline tracing the segmentation on the input image is overlaid in the segmentation of the CF image as well, confirming the reduction in predicted lung size. B) A plot showing the sum of pixels predicted as lung as the λ is changed during the Latent Shift CF generation process.

5. Experiments

5.1. Lung Size

In order to verify that this method works, an easily auditable CF can be generated for lung size. The work (Hofmanninger et al., 2020) released a lung segmentation model that we can transform into a regression task by taking the sum of the segmentation outputs for the lung class. As more pixels are classified as lung, the larger the sum will become. Figure 2A visualizes the CF generated for this task, demonstrating a strong visual signal that the lung size is reduced. Using that same model to segment the image and CF image, the size of the segmentation has been reduced. Here the segmentation is thresholded to 0.5 to make the comparison easier.

The reduction in lung size can also be validated by looking at the sum of the lung pixels (Figure 2B). We should observe that lowering the λ value reduces the total sum of pixels, which is what is observed. We do not observe an infinite monotonic reduction because the CF generation process is limited by the latent variable model’s ability to remove these features along the specific vector in the latent space identified by Latent Shift. Although it is more likely that a lung size smaller than what we achieve is outside the domain of the latent variable model and not something it can represent.

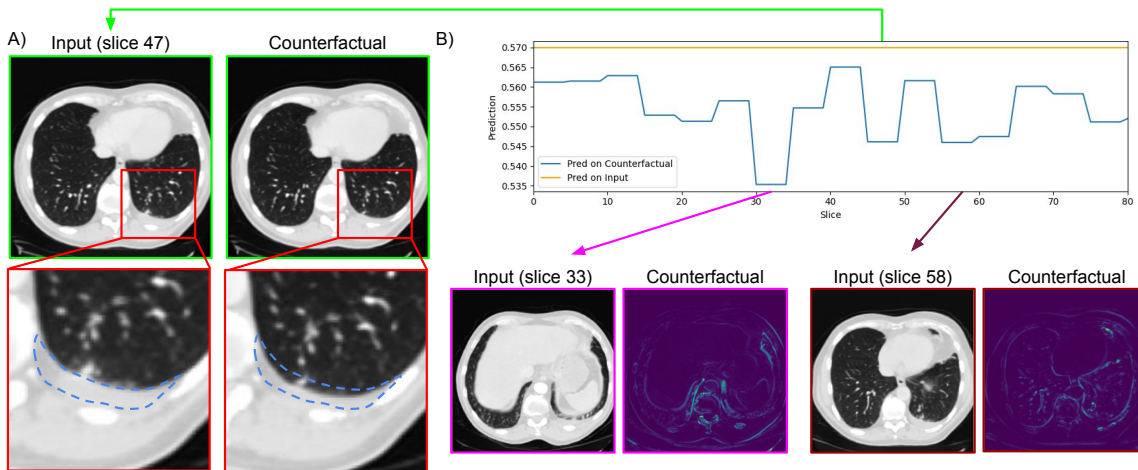


Figure 3: A: The input and CF slices showing a reduction in plural effusion. The blue dashed line outlines the side of the lung area that is reduced in the CF. B: Localization of CF slices that contribute to changes in the prediction. The volume is processed in chunks of five slices, restricting changes to that region. Slices between 30 and 35 are identified as producing the most change while slices 45-50 (Shown in A) and 55-60 also reduce the prediction. Heatmaps of these changes between the input and CF are shown.

5.2. Plural Effusion

Plural effusion, characterized by the accumulation of fluid between the pleural layers surrounding the lungs (Krishna et al., 2025), can be visually identified in CT scans as bright regions along the lung periphery. To validate that the classifier utilized in (Blankemeier et al., 2024) is using the correct features, we applied our counterfactual generation method to this task.

Figure 3A demonstrates the input and counterfactual (CF) slices, particularly at indices 33, 47, and 58. In these CF slices, reductions in the pleural effusion regions are visibly evident, outlined by dashed blue lines. This confirms that the generated counterfactuals correctly target the bright regions corresponding to fluid buildup, providing evidence that the classifier relies on appropriate features for its predictions.

To further analyze the classifier’s decision-making process, we localized the slices that contributed most significantly to changes in the prediction. Figure 3B shows heatmaps highlighting areas within slices where the differences between the input and CF are most pronounced. By processing the volume in chunks of five slices and restricting changes to specific regions, we identified slices 30-35, 45-50, and 55-60 as having the greatest impact on the prediction. For instance, slices 45-50, visualized in Figure 3A, exhibit substantial reduction in the pleural effusion region, aligning with a decrease in the classifier’s confidence.

6. Conclusion

In this work, we demonstrated the ability to generate counterfactual CT volumes using a slice-based VQ-VAE encoder-decoder architecture. Our approach effectively addresses the challenges of limited training data and high memory requirements associated with 3D medical imaging.

The case studies validate that the generated counterfactuals target clinically relevant features, highlighting the potential of this method for improving the transparency and trustworthiness of AI systems in medical applications. Furthermore, our approach allows for localized analysis, providing insights into the regions most influential to the classifier’s predictions. This capability highlights the potential of counterfactual explanations to enhance transparency and trust in AI systems, particularly in high-stakes medical applications.

7. Acknowledgments

We would like to thank Stanford University and the Stanford Research Computing Center for providing computational resources and support that contributed to these research results.

References

- Louis Blankemeier, Joseph Paul Cohen, Ashwin Kumar, Dave Van Veen, Syed Jamal Safdar Gardezi, Magdalini Paschali, Zhihong Chen, Jean-Benoit Delbrouck, Eduardo Reis, Cesar Truys, Christian Bluethgen, Malte Engmann Kjeldskov Jensen, Sophie Ostmeier, Maya Varma, Jeya Maria Jose Valanarasu, Zhongnan Fang, Zepeng Huo, Zaid Nabulsi, Diego Ardila, Wei-Hung Weng, Edson Amaro Junior, Neera Ahuja, Jason Fries, Nigam H. Shah, Andrew Johnston, Robert D. Boutin, Andrew Wentland, Curtis P. Langlotz, Jason Hom, Sergios Gatidis, and Akshay S. Chaudhari. Merlin: A Vision Language Foundation Model for 3D Computed Tomography. 2024. URL <https://arxiv.org/abs/2406.06512>.
- Joseph Paul Cohen, Rupert Brooks, Sovann En, Evan Zucker, Anuj Pareek, Matthew P. Lungren, and Akshay Chaudhari. Gifsplanation via Latent Shift: A Simple Autoencoder Approach to Counterfactual Generation for Chest X-rays. *Medical Imaging with Deep Learning*, 2021. URL <https://openreview.net/forum?id=rnunjvgxAMt>.
- Patrick Esser, Robin Rombach, and Björn Ommer. Taming transformers for high-resolution image synthesis. In *Computer Vision and Pattern Recognition*, 2021. ISBN 9781665445092. doi: 10.1109/CVPR46437.2021.01268. URL <http://arxiv.org/abs/2012.09841>.
- Johannes Hofmanninger, Forian Prayer, Jeanny Pan, Sebastian Röhrich, Helmut Prosch, and Georg Langs. Automatic lung segmentation in routine imaging is primarily a data diversity problem, not a methodology problem. *European Radiology Experimental*, 2020. ISSN 2509-9280. doi: 10.1186/s41747-020-00173-2. URL <https://eurradiolexp.springeropen.com/articles/10.1186/s41747-020-00173-2>.

- Rachana Krishna, Marsha H. Antoine, Mohamed H. Alahmadi, and Mohan Rudrappa. *Pleural Effusion*. StatPearls Publishing, 8 2025. URL <http://www.ncbi.nlm.nih.gov/pubmed/25077579>.
- Adam Paszke, Sam Gross, Francisco Massa, Adam Lerer, James Bradbury, Gregory Chanan, Trevor Killeen, Zeming Lin, Natalia Gimelshein, Luca Antiga, Alban Desmaison, Andreas Köpf, Edward Yang, Zach DeVito, Martin Raison, Alykhan Tejani, Sasank Chilamkurthy, Benoit Steiner, Lu Fang, Junjie Bai, and Soumith Chintala. PyTorch: An Imperative Style, High-Performance Deep Learning Library. *Neural Information Processing Systems*, 12 2019. URL <https://arxiv.org/abs/1912.01703>.
- Arnaud Arindra Adiyoso Setio, Alberto Traverso, Thomas de Bel, Moira S. N. Berens, Cas van den Bogaard, Piergiorgio Cerello, Hao Chen, Qi Dou, Maria Evelina Fantacci, Bram Geurts, Robbert van der Gugten, Pheng Ann Heng, Bart Jansen, Michael M. J. de Kaste, Valentin Kotov, Jack Yu-Hung Lin, Jeroen T. M. C. Manders, Alexander Sónora-Mengana, Juan Carlos García-Naranjo, Evgenia Papavasileiou, Mathias Prokop, Marco Saletta, Cornelia M Schaefer-Prokop, Ernst T. Scholten, Luuk Scholten, Miranda M. Snoeren, Ernesto Lopez Torres, Jef Vandemeulebroucke, Nicole Walasek, Guido C. A. Zuidhof, Bram van Ginneken, and Colin Jacobs. Validation, comparison, and combination of algorithms for automatic detection of pulmonary nodules in computed tomography images: the LUNA16 challenge. 2016. doi: 10.1016/j.media.2017.06.015. URL <http://arxiv.org/abs/1612.08012><http://dx.doi.org/10.1016/j.media.2017.06.015>.
- Mohammad A Thanoon, Mohd Asyraf Zulkifley, Muhammad Ammirul Atiqi Mohd Zainuri, and Siti Raihanah Abdani. A Review of Deep Learning Techniques for Lung Cancer Screening and Diagnosis Based on CT Images. *Diagnostics*, 2023. ISSN 2075-4418. doi: 10.3390/diagnostics13162617. URL <http://www.ncbi.nlm.nih.gov/pubmed/37627876><http://www.pubmedcentral.nih.gov/articlerender.fcgi?artid=PMC10453592>.
- Jakob Wasserthal, Hanns-Christian Breit, Manfred T. Meyer, Maurice Pradella, Daniel Hinck, Alexander W. Sauter, Tobias Heye, Daniel Boll, Joshy Cyriac, Shan Yang, Michael Bach, and Martin Segeroth. TotalSegmentator: robust segmentation of 104 anatomical structures in CT images. 2022. doi: 10.1148/ryai.230024. URL <http://arxiv.org/abs/2208.05868><http://dx.doi.org/10.1148/ryai.230024>.
- Ke Yan, Xiaosong Wang, Le Lu, and Ronald M. Summers. DeepLesion: Automated Deep Mining, Categorization and Detection of Significant Radiology Image Findings using Large-Scale Clinical Lesion Annotations. 2017. URL <http://arxiv.org/abs/1710.01766>.